Supporting Information for: Disentangling the ultrafast nonlinear optical behaviour of plasmonic resonances near the interband transition

Andrea Schirato Mychel G. Silva Danielle C. Teles-Ferreira Cristian Manzoni Ana Maria de Paula Giulio Cerullo Giuseppe Della Valle* Marcel Di Vece**

A. Schirato
Dipartimento di Fisica - Politecnico di Milano, Piazza Leonardo da Vinci, 32, I-20133 Milano, Italy
Istituto Italiano di Tecnologia, via Morego 30, I-16163, Genova, Italy
Dr. D. C. Teles-Ferreira
Instituto Federal de Minas Gerais, Campus Ouro Preto, Ouro Preto 35400-000, MG, Brazil
Dr. M. G. Silva, Prof. A. M. de Paula
Departamento de Física, Universidade Federal de Minas Gerais, 31270-901 Belo Horizonte, MG, Brazil
Dr. C. Manzoni
Istituto di Fotonica e Nanotecnologie - Consiglio Nazionale delle Ricerche, Piazza Leonardo da Vinci, 32, I-20133 Milano, Italy
Prof. G. Cerullo*
Dipartimento di Fisica - Politecnico di Milano, Piazza Leonardo da Vinci, 32, I-20133 Milano, Italy
Istituto di Fotonica e Nanotecnologie - Consiglio Nazionale delle Ricerche, Piazza Leonardo da Vinci, 32, I-20133 Milano, Italy
Email Address: giulio.cerullo@polimi.it
Prof. G. Della Valle*
Dipartimento di Fisica - Politecnico di Milano, Piazza Leonardo da Vinci, 32, I-20133 Milano, Italy
Istituto di Fotonica e Nanotecnologie - Consiglio Nazionale delle Ricerche, Piazza Leonardo da Vinci, 32, I-20133 Milano, Italy
Email Address: giuseppe.dellavalle@polimi.it
Prof. M. Di Vece*
CIMAINA and Dipartimento di Fisica, Università di Milano, Via Celoria 16, 20133 Milano, Italy
Email Address: marcel.divece@unimi.it

S1. Quasi-static plasmonic resonance modelling

To simulate the static optical response of the sample, we applied a reduced model which, to the leading order, neglects the polycrystallinity, size and shape dispersion of nanostructures (see Fig. S1) and describes them as an ensemble of monodisperse nanospheres. As mentioned in the main text, this assumption requires to introduce two fitting parameters, namely the surrounding refractive index n_{env} and the Drude damping factor Γ, in order to mimic the degree of cristallinity and inhomogeneous broadening of the actual sample and to provide a quantitatively accurate estimation of the static measurement. In this framework, the system absorbance can be computed starting from the optical behaviour of an individual nanosphere.
Moreover, given the average size of the nanocrystals in the sample (diameter $\bar{D} = 26.3$ nm), much smaller than the optical wavelengths λ, quasi-static theory (QST) can be applied to determine the nanostructure absorption, scattering and extinction cross-sections, σ_A, σ_S and σ_E respectively. Thus, by considering a monochromatic linearly polarised plane wave impinging on a sphere of radius $R \simeq \bar{D}/2$ and permittivity $\varepsilon_m(\lambda)$, embedded in a homogeneous medium with wavelength-independent dielectric constant $\varepsilon_d = n_{env}^2$, QST provides the analytical expression for the particle isotropic polarizability, $\alpha(\lambda)$, reading [1]:

$$\alpha(\lambda) = 4\pi R^3 \frac{\varepsilon_m(\lambda) - \varepsilon_d}{\varepsilon_m(\lambda) + 2\varepsilon_d}, \tag{S1}$$

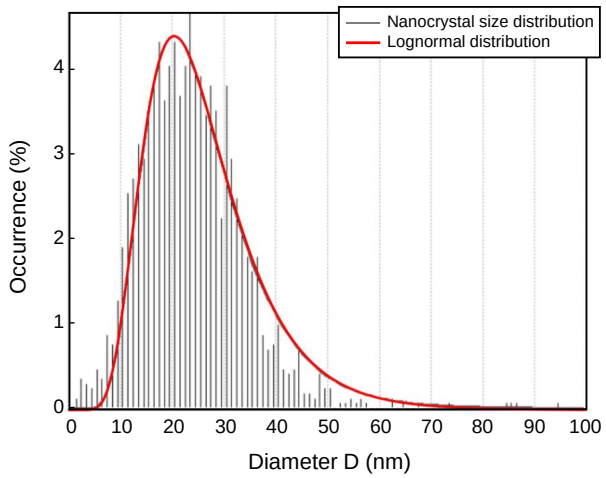

Figure S1: Gold nanocrystals size distribution obtained from TEM micrographs and approximated by a best-fit lognormal distribution (red solid line) with mean value $\bar{D} = 26.3$ nm and standard deviation 2 nm.

and associated to a point-like electric dipole $\mathbf{p} = \varepsilon_0 \varepsilon_d \alpha(\lambda) \mathbf{E}_0$, with $\mathbf{E}_0$ the incident (uniform) electric field. Note that at the denominator of $\alpha(\lambda)$ there is nothing but the expression setting the condition for the plasmonic resonance to occur, i.e. the Fröhlich condition. From the polarizability it is then possible to determine the absorption and scattering cross-sections, defined as $\sigma_A = P_A/I_0$ and $\sigma_S = P_S/I_0$, with P_A and P_S the total power absorbed and scattered by the nano-object, respectively, and $I_0 = \frac{1}{2}\sqrt{\varepsilon_d} c \varepsilon_0 |\mathbf{E}_0|^2$ the incident intensity. Calculations [1] lead to:

$$\sigma_A(\lambda) = k \mathrm{Im}\Big\{\alpha(\lambda)\Big\}, \tag{S2}$$

$$\sigma_S(\lambda) = \frac{k^4}{6\pi}\Big|\alpha(\lambda)\Big|^2, \tag{S3}$$

with $k = n_{env} 2\pi/\lambda$ the incident wave-number. The total extinction cross-section is then simply given by the sum $\sigma_E(\lambda) = \sigma_A(\lambda) + \sigma_S(\lambda)$. By considering the nanocrystal density per unit volume within the experimental sample ($n_p = 30$ nanoparticles/μm^2), Lambert Beer's law can be applied to estimate the sample transmission $T(\lambda) = \exp[-\sigma_E(\lambda) n_p]$, corresponding to an absorbance $A = -\log_{10}[T(\lambda)]$. For gold permittivity, a Drude-Lorentz analytical expression [2] fitted on experimental data [3] was adopted, where an increased Drude damping factor Γ, following the approach reported in [4], allowed us to reproduce the resonance inhomogeneous broadening (as detailed in the main text).

S2. Transient absorption spectroscopy measurements

To analyse the nonlinear modulation of the Au nanocrystal optical response at different excitation levels, transient absorption spectroscopy measurements have been performed by varying the pump pulse fluence. Figure S2 (panels a, c, e, g) shows experimental maps of the measured differential transmittance $\Delta T/T$ as a function of the probe wavelength and pump-probe time delay, obtained by exciting the sample with a pump pulse centred at 400 nm (as in the main text) for increasing values of the beam fluence, ranging from 84 μJ/cm^2 to 1.4 mJ/cm^2. We emphasize that, even when pumping with the highest fluence, the sample did not experience any permanent photoinduced damage. No melting was caused by pulse absorption, ensuring reproducibility of our experiments, as evidenced by unchanged optical transmission upon repeated measurements under the same conditions. This observation is in agreement with the estimation of the absorbed energy density per particle in our experimental conditions (~ 0.1 aJ/nm^3 when $F = 1.4$ mJ/cm^2), one order of magnitude smaller than the melting threshold reported for comparable nanostructures [5, 6]. Except for the pump fluence, the experimental conditions were identical for all the measurements. Specifically, the relative angle between the propagation directions of pump and probe was of $0.5° - 1°$, and the beams, with spot size ~ 250 μm, were cross-polarized.

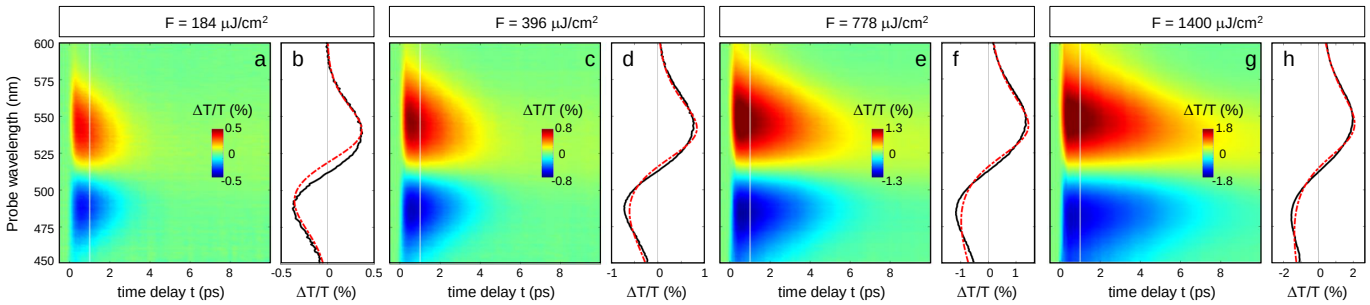

Figure S2: (a-h) Measured transient differential transmission maps (a, c, e, g), together with spectral sections evaluated at a time delay of 1 ps (solid black lines, highlighted as white vertical lines in the corresponding maps) and their Gaussian fit (dash-dotted red lines) (b, d, g, h) under varying pump laser fluence F, set respectively equal (from left to right) to 184 μJ/cm^2 (a, b); 396 μJ/cm^2 (c, d); 778 μJ/cm^2 (e, f); 1400 μJ/cm^2 (g,h). Vertical white lines in (a) and (b) identify the 1-ps time delay.

Importantly, the results of the experiments were then fitted (following the procedure outlined in the main text) in order to extract the trend of the fitting parameters as a function of fluence reported in the text (Fig. 4) and to systematically investigate the origin of the negative derivative shape observed in the transient maps. Therefore, as for the data in the main text, Fig. 3, spectral sections of the entire set of measurements were evaluated at a time delay of 1 ps and fitted according to Eq. (1) in the text. Figure S2b, S2d, S2f, S2h show a direct comparison between the experimental (solid black lines) and fitted data (dash-dotted red lines). The results of the fit confirm that, regardless of the pump fluence, the experimental spectra are well reproduced by a difference between two Gaussian profiles. However, to achieve a good agreement, the fitting algorithm requires letting all the five parameters (amplitudes, peak positions and background extinction) vary, namely it does not consider a blue shift as the only mechanism in place during the ultrafast optical modulation.

S3. Transient absorption spectroscopy modelling

The transient optical model employed to simulate the ultrafast nonlinear response observed experimentally has been outlined in the main text. It relies on the Three-Temperature Model (3TM) [7] to describe the energy relaxation processes following the pump photoabsorption (in terms of the three variables N, Θ_E and Θ_L) and, in cascade, it combines the time-dependent solution of the 3TM with a semi-classical modelling of the thermo-modulational nonlinearities in Au [8, 9] to determine the pump-induced transient changes in the metal permittivity, driving the optical modulation. Detailed discussions on the 3TM implementation are reported elsewhere [9, 10]. Regarding the photoinduced permittivity variations, as mentioned in the main text, we accounted for both interband (due to modifications of the electron energy distribution given by N and Θ_E) and intraband (due to an increase in the Au lattice temperature, affecting the Drude term of the metal permittivity) contributions, in agreement with previous reports (refer e.g. to [9, 10, 11] and references therein). More in detail, for the terms of the permittivity change due to out-of-equilibrium electrons, $\Delta\varepsilon_N$ and $\Delta\varepsilon_{\Theta_E}$, the modulation of both the L and X transitions have been included in the calculations, under parabolic band approximation [8, 12]. On the other hand, an increased lattice temperature drives a modulation of the intraband permittivity term, resulting from a modification the Drude damping and the plasma frequency. In general, the heating of the lattice (taking place in the 10s-100s ps timescale) can also excite acoustic oscillations, giving rise to a modulation (at the acoustic frequency) of the nanostructure optical response, which can be observed in the transient optical signal. This effect has been the subject of extensive research, aimed at both measuring and gaining insight on the vibrational mechanisms triggered by light absorption [9, 13, 14, 15, 16, 17]. However, the period of mechanical vibrational modes of Au nanoparticles of 20-30 nm in size is typically 2-3 times longer than the time scale of interest in the present study, which is rather that of electron-phonon relaxation, requiring ∼10 ps [14]. Therefore, if present, acoustic oscillations are expected to provide a negli-

gible contribution to the transient optical response on the here considered time scale, dominated by the thermo-modulational nonlinearity of hot electrons. Moreover, due to the size and shape dispersion of our sample, mechanical oscillations are not expected to contribute to the signal modulation, even at longer time delays. Indeed, nanostructures with different sizes translate into mechanical resonances with different oscillation periods. The ensemble response, superposition of each contribution, would be too broadened to allow for observing well-defined oscillations. This justifies our choice not to include such effect in the modelling. A comprehensive discussion of our model implementation can be found e.g. in [18], while the values of the band parameters (energy gaps from the Fermi level and electron effective masses) used in the present work, either taken or adapted from refs [12, 19], are reported in Table S1.

	E_{0v} (eV)	E_{0c} (eV)	$m_{v\perp}/m_0$	$m_{c\perp}/m_0$	$m_{v\parallel}/m_0$	$m_{c\parallel}/m_0$
X	1.650	1.475	0.770	0.220	0.814	0.180
L	1.575	0.717	0.720	0.190	0.774	0.260

Table S1: Band parameters for the X and L interband transitions in Au used in our calculations (m_0 being the free electron mass).

We emphasize that our modelling approach, combining the 3TM with the semiclassical description of Au nonlinearities, does not apply exclusively to the case of interband excitations investigated in the present work. Indeed, we employed it for intraband excitations as well, i.e. when the pump photon energy is below the threshold for interband transitions. For instance, this has been done by some of the authors in ref. [9], where single Au nanorods were pumped at 780 nm. Moreover, we performed a direct comparison between intraband (800-nm pump wavelength) and interband (400-nm pump wavelength) excitation for Au nanorods dispersed in water [20] as well as Au nanocrosses in metasurface configuration [21], proving the accuracy of the model in both conditions. Previous studies also demonstrated the marginal impact of the excitation wavelength on the transient optical response, provided that similar excitation conditions (and in particular, comparable absorbed pump fluence) are used. More recently, we have however predicted that, in suitable conditions (high aspect ratio nanostructures, where local spatial inhomogeneities of the excitation become relevant), different dynamics of the probe signals can be induced, depending on the pump photon energy [22]. A similar observation has been reported for a quasi-2D array of Au nanoellipsoids, by isolating the purely non-thermal contribution to their ultrafast dynamics [23]. The effect is due to the dependence on the pump photon energy of the spectral dispersion of the permittivity modulation driven by the non-thermal carrier distribution N. In the present case, however, non-thermal carriers contribute to a lesser degree to the overall transient signal (refer to Fig. 5 of the main text), making the impact of the excitation wavelength mostly negligible. Once the spectrally dispersed and complex-valued permittivity changes are computed as a function of probe wavelength and time, the transient response of the system can be determined. The calculation of the dynamical extinction cross section under QST approximation follows precisely the approach discussed in S1 for the static conditions, yet considering a transiently modified metal permittivity $\varepsilon_{tr}(\lambda, t) = \varepsilon_m(\lambda) + \Delta\varepsilon(\lambda, t)$ which gives rise to a differential extinction cross-section $\Delta\sigma_E(\lambda, t)$. As a final step of the model, the transient transmittance spectra are calculated as follows:

$$\frac{\Delta T}{T}(\lambda, t) = \exp\Big[-\Delta\sigma_E(\lambda, t)n_p\Big] - 1, \tag{S4}$$

which directly compares with the measured signal.
On the other hand, to disentangle the experimental differential transmittance signal into the terms arising from different mechanisms of the permittivity modulation (as reported in Fig. 5 of the main text), the same calculations are performed starting from the corresponding contribution of interest, namely the real or imaginary part of either $\Delta\varepsilon_N$, $\Delta\varepsilon_{\Theta_E}$ or $\Delta\varepsilon_{\Theta_L}$, instead of the total $\Delta\varepsilon$, sum of each of these terms.

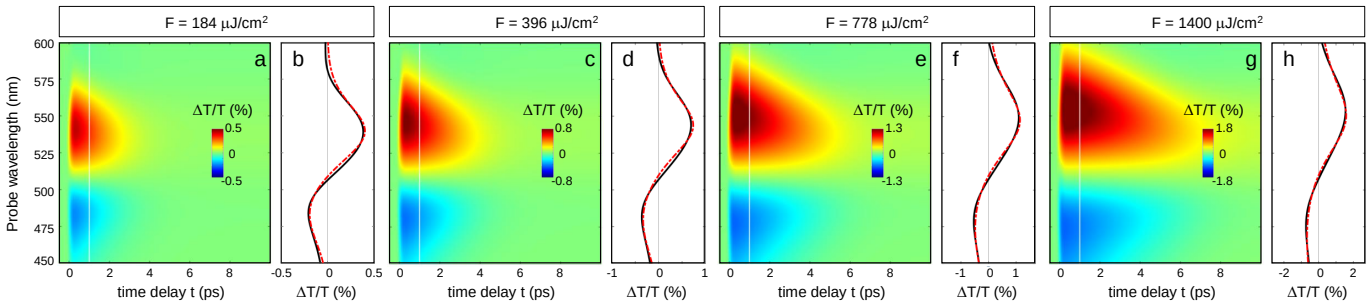

Figure S3: (a-h) Simulated transient differential transmission maps (a, c, e, g), together with spectral sections evaluated at a time delay of 1 ps (solid black line, highlighted as white vertical lines in the corresponding maps) and their Gaussian fit (dash-dotted red line) (b, d, g, h) under varying pump laser fluence F, set respectively equal (from left to right) to 184 μJ/cm^2 (a, b); 396 μJ/cm^2 (c, d); 778 μJ/cm^2 (e, f); 1400 μJ/cm^2 (g,h). Vertical white lines in (a) and (b) identify the 1-ps time delay.

Moreover, as for experiments, we performed numerical simulations by varying the pump pulse fluence. Figure S3 reports the computed maps of the $\Delta T/T$ signal, in good agreement with the corresponding experiments (compare same panels in Fig. S2). This does not hold exclusively for the $\Delta T/T$ spectra, but also for its dynamics. To better visualize the latter, Figure S4 reports the (normalized) temporal sections of both experimental and numerical maps at a wavelength of 550 nm (close to the signal positive peak). Comparing them for the same pump fluence indicates that the measured signal decay, dictated by the electron relaxation due to scattering with phonons, indeed compares well with the simulated $\Delta T/T$ signal.

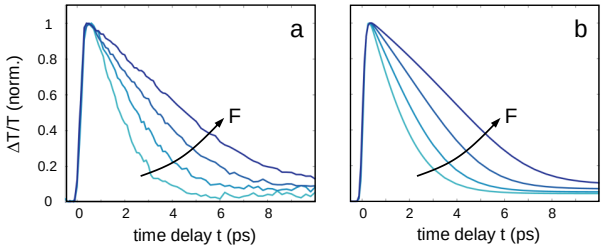

Figure S4: (a) Normalized temporal section of the experimental and (b) simulated $\Delta T/T$ at a selected wavelength of 550 nm, under varying increasing pump laser fluence F, set to 184 μJ/cm^2; 396 μJ/cm^2; 778 μJ/cm^2; 1400 μJ/cm^2 from lighter to darker colour shade.

In Fig. S3, the numerical differential transmission maps are presented together with the results of the fitting procedure carried out on simulated data, which are shown to be well fitted by a double-Gaussian. Likewise, the fit analysis performed on experimental data (Fig. 4 of the main text) was also extended to numerical spectra. The fitting parameters of Eq. (1) were studied for the entire set of simulations (Fig. S3), to extract their trend as a function of the pump fluence.

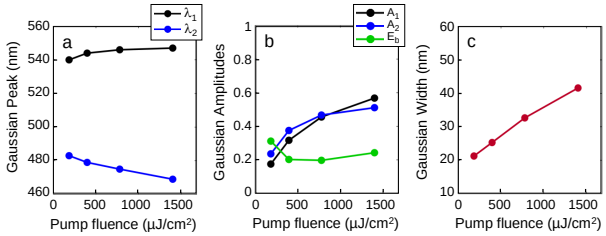

Figure S5: (a) Peak position $\lambda_{1,2}$, (b) amplitude $A_{1,2}$ and (c) width w of the two Gaussian profiles of Eq. (1), retrieved when fitting the simulated differential transmittance signal $\Delta T/T$ at 1 ps time delay by varying the pump fluence. The fitted background level E_b (green) is also shown in panel (b).

The outcome of our analysis is reported in Fig. S5, showing the evolution of the peak positions, ampli-

tudes and width of the fitting Gaussian profiles, alongside the non-resonant background E_b. The obtained trend compares well with the fitting of the experimental $\Delta T/T$ spectra (Fig. 4), demonstrating that also when fitting simulated spectra, all the six parameters of Eq. (1) exhibit a strong dependence on the pump fluence. This further corroborates the inadequacy of the fitting procedure to fully explain the physical phenomena underlying the observed transient maps.

References

[1] S. A. Maier, *Plasmonics: fundamentals and applications*, Springer Science & Business Media, **2007**.

[2] P. G. Etchegoin, E. C. L. Ru, M. Meyer, *The Journal of Chemical Physics* **2006**, *125*, 16 164705.

[3] P. B. Johnson, R. W. Christy, *Physical Review B* **1972**, *6*, 12 4370.

[4] M. Husnik, S. Linden, R. Diehl, J. Niegemann, K. Busch, M. Wegener, *Phys. Rev. Lett.* **2012**, *109* 233902.

[5] X. Hou, N. Djellali, B. Palpant, *ACS Photonics* **2018**, *5*, 9 3856.

[6] S. Link, M. A. El-Sayed, *The Journal of Chemical Physics* **2001**, *114*, 5 2362.

[7] C.-K. Sun, F. Vallée, L. H. Acioli, E. P. Ippen, J. G. Fujimoto, *Physical Review B* **1994**, *50*, 20 15337.

[8] R. Rosei, *Physical Review B* **1974**, *10*, 2 474.

[9] M. Zavelani-Rossi, D. Polli, S. Kochtcheev, A.-L. Baudrion, J. Béal, V. Kumar, E. Molotokaite, M. Marangoni, S. Longhi, G. Cerullo, P.-M. Adam, G. Della Valle, *ACS Photonics* **2015**, *2*, 4 521.

[10] A. Schirato, M. Maiuri, A. Toma, S. Fugattini, R. Proietti Zaccaria, P. Laporta, P. Nordlander, G. Cerullo, A. Alabastri, G. Della Valle, *Nature Photonics* **2020**, *14*, 12 723.

[11] S. Dal Conte, M. Conforti, D. Petti, E. Albisetti, S. Longhi, R. Bertacco, C. De Angelis, G. Cerullo, G. Della Valle, *Physical Review B* **2014**, *89*, 12 125122.

[12] M. Guerrisi, R. Rosei, P. Winsemius, *Physical Review B* **1975**, *12*, 2 557.

[13] G. V. Hartland, *Annual Review of Physical Chemistry* **2006**, *57*, 1 403.

[14] G. V. Hartland, *Chemical Reviews* **2011**, *111*, 6 3858, pMID: 21434614.

[15] A. Crut, P. Maioli, N. D. Fatti, F. Vallée, *Physics Reports* **2015**, *549* 1.

[16] A. Ahmed, M. Pelton, J. R. Guest, *ACS Nano* **2017**, *11*, 9 9360.

[17] T. O. Otomalo, L. D. Mario, C. Hamon, D. Constantin, F. Toschi, K.-V. Do, V. Juvé, P. Ruello, P. O'Keeffe, D. Catone, A. Paladini, B. Palpant, *Chemosensors* **2022**, *10*, 5 193.

[18] A. Marini, M. Conforti, G. Della Valle, H. Lee, T. X. Tran, W. Chang, M. Schmidt, S. Longhi, P. S. J. Russell, F. Biancalana, *New Journal of Physics* **2013**, *15*, 1 013033.

[19] N. E. Christensen, B. Seraphin, *Physical Review B* **1971**, *4*, 10 3321.

[20] M. G. Silva, D. C. Teles-Ferreira, L. Siman, C. R. Chaves, L. O. Ladeira, S. Longhi, G. Cerullo, C. Manzoni, A. M. de Paula, G. Della Valle, *Physical Review B* **2018**, *98*, 11 115407.

[21] A. Schirato, A. Toma, R. P. Zaccaria, A. Alabastri, G. Cerullo, G. D. Valle, M. Maiuri, *Advanced Optical Materials* **2022**, *10*, 10 2102549.

[22] A. Schirato, G. Crotti, R. P. Zaccaria, A. Alabastri, G. D. Valle, *New Journal of Physics* **2022**, *24*, 4 045001.

[23] P. O'Keeffe, D. Catone, L. D. Mario, F. Toschi, M. Magnozzi, F. Bisio, A. Alabastri, R. P. Zaccaria, A. Toma, G. D. Valle, A. Paladini, *Laser & Photonics Reviews* **2021**, *15*, 6 2100017.